Size effect and electrical ageing of PDMS dielectric elastomer with competing failure modes

Emmanuel Taine[1,2], Thomas Andritsch[1], Istebreq A. Saeedi[1] and Peter H. F. Morshuis[3]

[1] The Tony Davies High Voltage Laboratory, University of Southampton, Southampton, UK
[2] Research & Development Laboratory, SBM Offshore, Carros, France
[3] Solid Dielectric Solutions, Leiden, The Netherlands

E-mail: et7n21@soton.ac.uk

Received xxxxxx
Accepted for publication xxxxxx
Published xxxxxx

Abstract

Large-scale dielectric elastomer generators DEGs such as those employed in wave energy converter projects require a significant volume of electrically stressed materials. Meanwhile, predictions of energy output from such systems are generally extrapolated from electrical and mechanical breakdown measurements performed on small scale samples, where the presence of small defects can be extremely small. This can lead to overly optimistic upscaled predictions for the performance and reliability of full-scale devices. In this study, multilayer DEGs were prepared to evaluate the dielectric breakdown strength of thin polydimethylsiloxane PDMS elastomer at different values of active areas. The results indicated the presence of two separate breakdown mechanisms resulting in an enhanced size effect and a reduced reliability for the larger samples. Electrical ageing tests were performed on three different sample geometries and the dielectric breakdown strength was found to be marginally affected by the time under stress. A Weibull competing failure model was applied to the distribution of experimental breakdowns and electrical reliability was accurately modelled over more than 4 decades of variation in the electrode area.

Keywords: Dielectric breakdown strength; size effect; electrical ageing; PDMS; competing failure mode

1. Introduction

Dielectric elastomer generators (DEGs) are soft transducers capable of converting mechanical energy into electrostatic energy. They consist of a thin dielectric elastomer film sandwiched between two compliant electrodes, resulting in a stretchable capacitor. The DEG is stretched by an external mechanical force (*A* to *B* in Figure 1), and a voltage is applied across the electrodes when the stretch is maximal (*C*). The release of external mechanical force leads to a decrease in the electrical capacitance and an increase in the electrostatic energy (*C* to *D*). The stretchability of DEGs makes them particularly suitable for large strain amplitudes oscillating at low frequency. DEGs have been proposed in a variety of applications such as human body motions [1, 2], wave energy converters [2-6] or other types of vibrational environments [7, 8].

Energy densities higher than 1 $J.g^{-1}$ are theoretically achievable with DEGs [9-11]. These attractive numbers are generally obtained when considering materials operated at their intrinsic limits (namely the dielectric breakdown strength and the strain at break). However, in practical or commercial applications, the transducer will have to be operated well away from its critical points in the interest of reliability [12]. Electrical limits are known to change with the elastomer

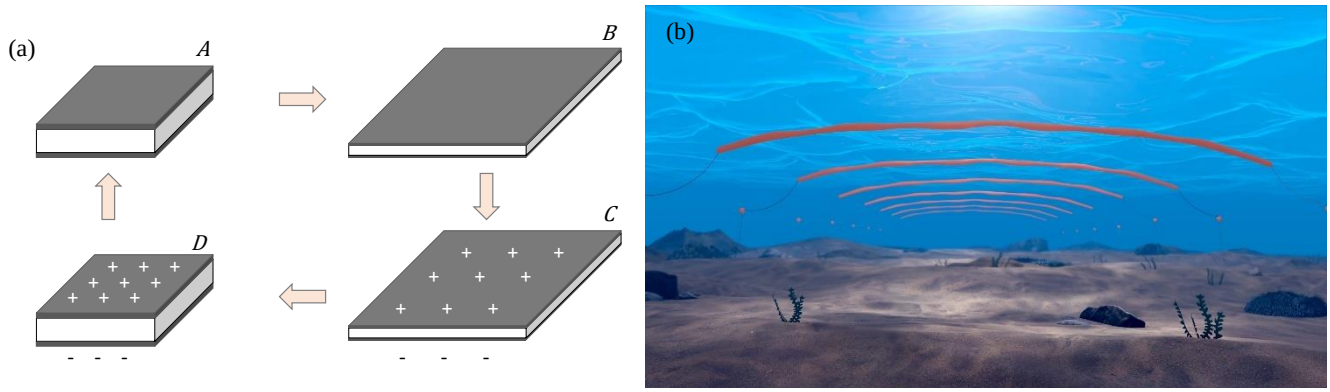

Figure 1. Working principle of a DEG (a) and its potential application in a wave energy converter farm (b).

stiffness [13-15], amount of pre- stretch [16-18], dielectric thickness [19, 20] and time under electrical stress [17]. The volume of elastomer that is electrically stressed also plays a role in the determination of the dielectric breakdown strength [18]. The latter is of prime importance in large-scale DEG systems such as the one represented in Figure 1(b), where several tons of dielectric elastomer are required for future commercial applications. The probability of finding a defect is growing with the volume of stressed material, leading to a reduced effective breakdown strength for these larger volumes. This is known as *the weakest link theory* or *the volume effect*. Although, it has been widely investigated for power cable insulation [21-23] and high voltage capacitors [24-26], it remains unexplored when large volumes of dielectric elastomer are involved. Upscaling of materials and manufacturing strategies are seen as crucial milestones to address to make DEG a viable option for energy conversion [6, 27] and, according to [28], building full-scale prototypes represents an urgent challenge. This paper aims at highlighting the main obstacle of volume enlargement and addresses a novel methodology to capture the *size effect* in a reliability model in the presence of multiple failure mechanisms.

To study the sensitivity of dielectric breakdown strength to size variations, it is relatively straightforward to change the surface area of the electrodes while maintaining the thickness constant. However, due to space and budget limitations, this approach generally results in volume variations that remain within the same order of magnitude, making extrapolations to much larger volumes unreliable. In this paper, three sample geometries have been evaluated and a novel multilayer assembly has been developed, allowing the active surface to be increased by more than 4 decades from the smaller to the larger sample configuration. The resulting dielectric elastomers reached an active area of 35 m^2, which constitutes, to our knowledge, the largest upscaling reported. Detection of failure modes that remain hidden in classical breakdown experiments have been identified on these larger samples. A statistical approach using competing failure mode (CFM) analysis was combined to a Weibull weakest link model to predict the electrical reliability over the entire range of electrode areas evaluated. The model agrees very well with the experimental breakdown measured on the various sample sizes evaluated.

Lifetime is another important feature of large-scale DEGs. Using an accelerated life testing protocol, the sensitivity to electrical ageing was measured for the different specimen sizes. The CFM model was then modified to include time-induced electrical degradation. This methodology accurately described the experimental breakdowns at various specimen sizes, electric field, and exposure times, providing one single reliability function that can further guide the design of DEGs. The outcome of this work also allows for the evaluation of the relative importance of the different degradation variables. In future work, it can be used to address the variables that contribute the most to the reduction in energy density and reliability of large-scale DEGs.

2. Background

Reliability functions are widely employed to model experimental failures and improve availability of materials, components, or machines. The cumulative distribution function $U(x)$ represents the population fraction that failed at a given stress x (*e.g.* the electric field). The probability of survival $R(x)$ beyond stress x is the complement of the cumulative distribution function (1).

$$R(x) = 1 - U(x) \tag{1}$$

Many products come in various sizes, and their lifetimes are proportional to their volume. This is typically the case for capacitors or cable insulation, where lifetime is determined by the weakest portion of its dielectric [29]. These products can be regarded as a series of k sub-elements of volume Ω_0, such that the volume of the entire product is $\Omega = k\Omega_0$. For a system composed of k statistically independent components having the same reliability function $R_0(x)$, the system reliability

function is given by equation (2) [29].

$$R(x) = [R_0(x)]^k \quad (2)$$

High-voltage capacitors or DEGs, employ thin dielectric films where thickness variations are known to change the charge dynamics, resulting in local field enhancement [30]. Hence, a variation in thickness can change the breakdown strength because of two separate causes: a varying probability of finding a defect and localised field enhancement. As a result, the *size effect* in this paper is solely described by varying the electrode area (*A*) while holding the dielectric thickness (d_0) constant. Equation (2) is modified accordingly resulting in the cumulative distribution function described by (3) with A_0 the active electrode area of a reference sub-element.

$$U(x) = 1 - [R_0(x)]^{A/A_0} \quad (3)$$

From a statistical standpoint, equation (3) shows that unreliability increases with increased area: the probability of finding a defect causing premature failure increases as the area of stressed material increases. This *size effect* was already identified as an important feature to consider in the electrical breakdown strength evaluation of PDMS elastomers, even for small volume variations [18].

The Weibull distribution [31] is particularly well suited to describe extreme events and is widely employed in the lifetime prediction of electrical components. The cumulative distribution function (*cdf*) of a 2-parameter Weibull distribution is given in (4) with x the measured variable, η the scale parameter of the Weibull distribution (value at the 63.2^{th} percentile). The shape parameter β is the slope of the distribution on a bi-logarithmic scale and is a measure of the dispersion in the experimental data.

$$U(x) = 1 - e^{-\left(\frac{x}{\eta}\right)^{\beta}} \;;\; x \geq 0 \quad (4)$$

In many products, different failure modes are competing in the system, and a simple Weibull distribution is insufficient to model the experimental results. More sophisticated mixed distributions, such as multimodal Weibull or competing risks analysis, are required [32]. Typical examples include characterization of electrical breakdown in capacitor films [24] or mechanical characterization of fibres whose strength is determined by a competition among the strength distributions of defect sub-populations [33].

In this paper, the competing failure mode analysis has been used as it was found to better model the distribution of experimental breakdown, especially when the *size effect* was considered. Assuming a system subject to *N* independent competing failure causes, each distributed according to a Weibull distribution, the resulting *cdf* is of the form:

$$U(x) = 1 - \prod_{i=1}^{N} e^{-\left(\frac{x}{\eta_i}\right)^{\beta_i}} \;;\; x \geq 0 \quad (5)$$

where η_i and β_i are the scale and shape parameters of the i^{th} failure mode.

Stressed volume and electric field strength E are often mentioned as parameters affecting electrical unreliability U_e. Additionally, the service life of a material is ultimately defined by the stress levels imposed and their duration or repetitions. The long exposure time under electrical stress can induce a time dependent breakdown mechanism caused by space charge accumulation or thermal runaway. If the lifetime L is inversely proportional to the γ^{th} power of the electric field, the degradation is considered to obey the inverse power law (6) which is widely employed for lifetime estimation of electrical components [29]. K and γ are the model parameters which are experimentally determined. The power exponent γ is obtained from the slope of a bi-logarithmic plot of lifetime *vs.* electrical stress and measures the sensitivity to electrical ageing (a high γ value is desirable for the long-term reliability).

$$L(E) = KE^{-\gamma} \quad (6)$$

If time (t) is considered as the variable of the Weibull distribution in (4), and if the scale parameter of time to failures obeys to the inverse power law, the unreliability function U_0 of a reference specimen is given in equation (7) with $\beta_E = \gamma\beta_t$ and $K = {\eta_E}^{\gamma}\eta_t$. In this expression, β_E and β_t are the shape parameters of the experimental electric field and lifetime distributions, η_E and η_t the respective scale parameters.

$$U_0(E,t) = 1 - e^{-\left(\frac{E}{\eta_E}\right)^{\beta_E}\left(\frac{t}{\eta_t}\right)^{\beta_t}} \quad (7)$$

3. Method

3.1 Materials

The dielectric elastomer used was a two-component liquid silicone rubber (LSR) with 70 ShA Shore hardness. The LSR was diluted with a volatile silicone fluid in a LSR:solvent mixing ratio of 10:8 (determined from the mass). The product was mixed and degassed with a turbine mixer in a vacuum environment (~100 mbar). The resulting mixture was coated on a polymer carrier film using a roll-to-roll coater in a clean room environment fulfilling the ISO8 requirement. A first heating in a ventilated oven was done at 110 °C for a duration of 10 minutes to evaporate the solvent and to crosslink the elastomer. Final membrane thickness d_0 was measured at 145±5 µm with a digital microscope (Figure 2). Then, a compliant electrode made of a commercially available conductive LSR was coated over the dielectric PDMS layer

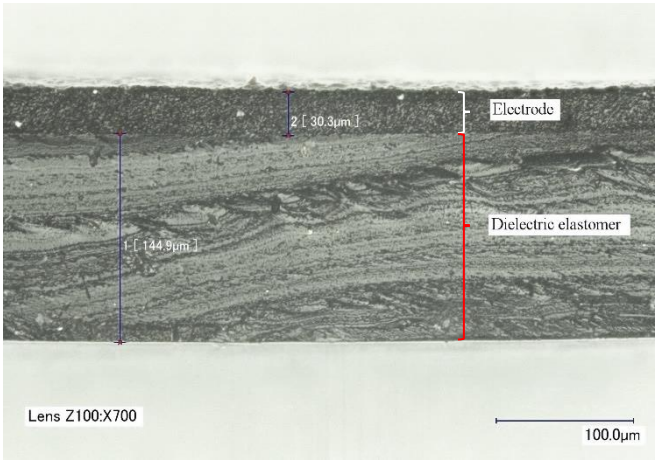

Figure 2. Section cut of the dielectric film and electrode (stripes in the dielectric layer are resulting from the cutting operation).

using a roll coater whose final thickness was measured at 30±5 µm. Finally, the elastomer stack was peeled from the carrier web, and a final post-curing was performed at 120 °C for a duration of 15 hours to eliminate the solvent residuals.

3.2 Samples preparation

In this study, three different electrode areas A have been evaluated, where the thickness of the dielectric layer remains unchanged between each geometry (Figure 3). The value of each active area was determined from equation (8) with C_0 the electric capacitance at rest (measured at 25 Hz), ε_0 the vacuum permittivity $\varepsilon_0 = 8.85 \times 10^{-12}$ F.m^{-1} and ε_r the relative permittivity of the dielectric elastomer (for the PDMS used in this study, a value of ε_r =2.7 has been measured). The active areas measured are given in Table 1 for each sample configuration, and the corresponding stressed volumes are schematically represented (with diagonal dashed regions) in Figure 3.

$$A = \frac{C_0 d_0}{\varepsilon_0 \varepsilon_r} \tag{8}$$

Results for the smaller area A_0 are obtained using a stainless-steel electrode constituted of a 40 mm diameter cylinder for which all edges have been rounded to a 3.4 mm radius, as represented in Figure 3(a). This electrode is connected to ground and is actuated by a 3-axis motor, allowing to test at different locations on a sample. The cylinder is positioned on the dielectric elastomer such, that only its mass contributes to the contact pressure at the film interface (4.3 kPa). The conductive compliant electrode, represented in black in Figure 3(a), is in contact with a mirror-polished stainless-steel plate, the latter being connected to the high voltage (HV) output of an external DC power supply (Heinzinger PNC 30kV). This testing configuration constitutes the reference case in this paper.

The sample is immersed in a silicone oil to prevent flashovers, and a polycarbonate frame is installed surrounding the cylindrical electrode to fix the position of the sample and prevent its displacement towards the vertical surface of the cylinder when the electric field is applied. Subsequently, a positive DC voltage V is applied across the dielectric elastomer using a constant ramp that can be adjusted from $r = 0.05\ \mathrm{V.s^{-1}}$ to $r = 5\ \mathrm{kV.s^{-1}}$. The corresponding electric field E is determined from the initial dielectric thickness as $E=V/d_0$. The breakdown voltage V_{BD} is detected from a sharp increase in the current measurement, and the corresponding dielectric breakdown strength is calculated from equation (9) using the initial film thickness. Hence, the dielectric thickness reduction induced by the electrostatic pressure is disregarded in the evaluation of the dielectric breakdown strength.

$$E_{BD} = V_{BD}/d_0 \tag{9}$$

Then, the vertical axis motor lifts the ground electrode and automatically moves to the next testing location, where the operation is repeated. A maximum of 24 equally distributed measurement points can be determined on a sheet of dielectric elastomer, as represented in Figure 3(a).

The area A_1 is obtained by testing the same film with the dielectric layer in contact with the stainless-steel plate on one side and the grounded rectangular conductive silicone on the other side, as illustrated in Figure 3(b). The resulting area covered by overlapping electrodes is increased by a factor of 78 compared to the reference area A_0.

Finally, the larger area A_2 is composed of a cylindrical capacitive stack that is obtained from a continuous winding process. Two dielectric films are simultaneously coated with electrodes before being assembled on a rotating mandrel to form the multi-layer assembly presented in Figure 3(c). In this geometry, the two electrodes are offsetted in the coating process such as the grounded electrode is ending on one extremity of the tubular stack, whereas the electrode connected to HV output is connected at the other extremity. Further details on the electrodes and dielectric arrangement have been described by van Kessel *et al.* [34]. Inner radius of the capacitor is fixed to $R = 100$ mm and the active width to 350 mm. The active area can be adjusted by changing the number of dielectric elastomer layers in the capacitive stack.

Table 1. Active area measured for each sample geometry.

Area	Symbol	Value	Unit	A/A_0
Reference	A_0	1.2×10^{-3}	m^2	1
Film	A_1	9.1×10^{-2}	m^2	78
Ring	A_2	3.5×10^{1}	m^2	2.9×10^{4}

3.3 Progressive stress test

Electronic components typically exhibit a high mean lifetime before failure. Therefore, life testing under operating

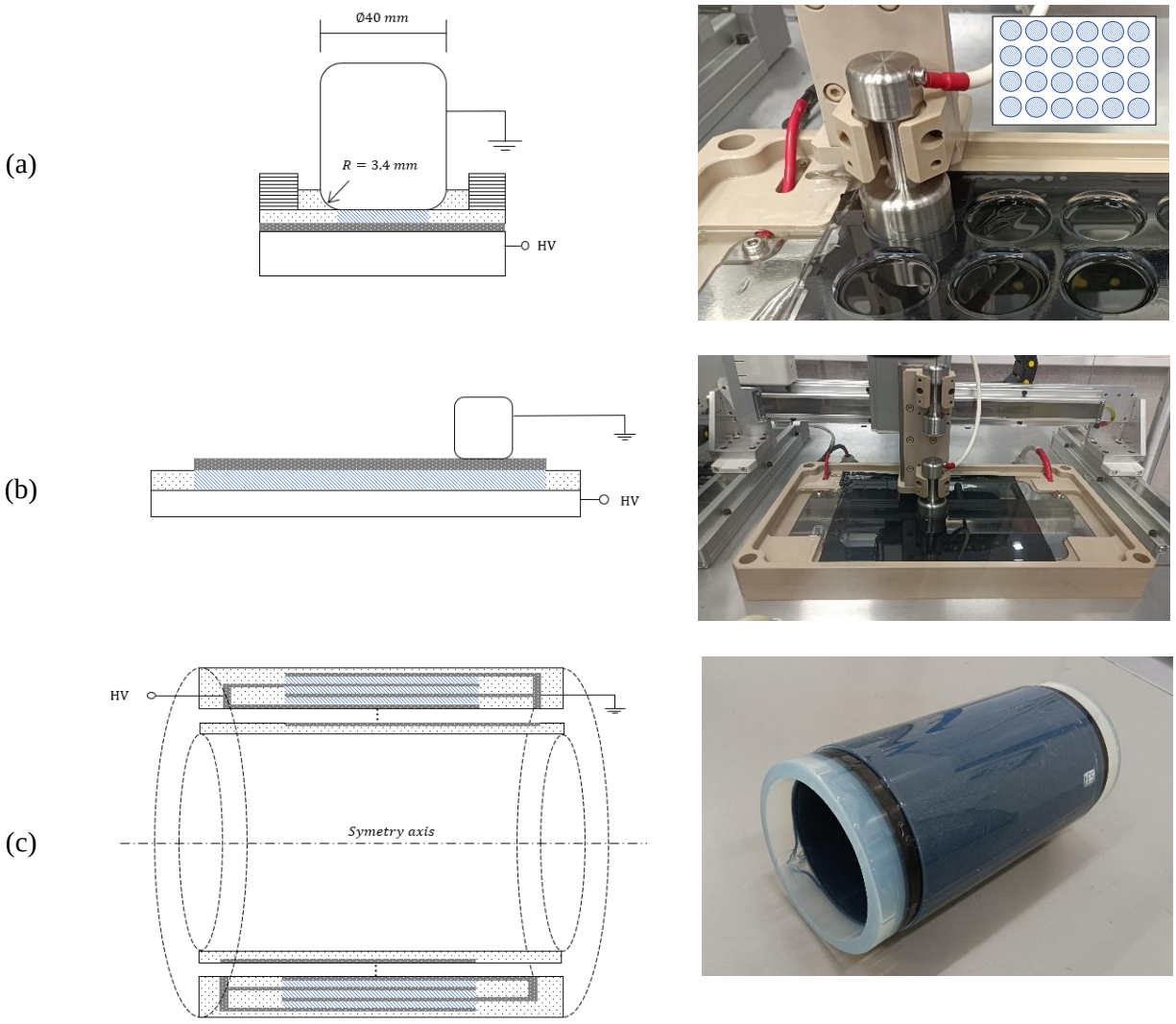

Figure 3. Samples geometries with the insulating PDMS dielectric layers represented in white with black dots, the compliant electrodes in grey with white dots, the volume of dielectric material electrically stressed with diagonal dashed lines for (a) the active area $\boldsymbol{A = A_0}$, (b) $\boldsymbol{A = A_1}$ and (c) $\boldsymbol{A = A_2}$. Geometries are representational only and not to scale.

conditions would be extremely time consuming. Different methodologies have been developed to reduce testing times and approximate lifetime in a reasonable resource. Accelerated Life Testing (ALT) is widely used to determine the failure time distribution of a product and the associated life-stress relationship in order to predict the product's long-term reliability under normal operating conditions. A step stress test methodology can be employed, which consists in placing a sample on test at a relatively mild stress level for a fixed time period. At the end of this period, the parts are inspected for failure, and the ones that have not failed are put back on test at the next higher stress level. They are tested for the same time period, and the procedure is repeated, until either a desired percentile or the total sample population fails. Voltage, temperature, and the length of the time interval of stress application are frequently used variables in the test program [35]. A variation of this ALT method is known as the progressive stress test. It is similar to the step stress test, where the time increment approaches zero and the rate of voltage increase is $r = \frac{dV}{dt}$. Testing at different rates will expose the sample to different times under stress, and the electrical damage D accumulated after an exposure time τ is given in equation (10) [35].

$$D = \int_0^{\tau} E(t)^{\gamma} dt = \left(\frac{r}{d_0}\right)^{\gamma} \int_0^{\tau} t^{\gamma} dt \qquad (10)$$

Integration of equation (10) leads to the inverse power law, and the sample fails once the accumulated damage reaches the critical damage value D_c after an exposure time τ_c representing its lifetime at a specific stress rate

(equation (11)). γ is the power exponent obtained from a plot of the electric field-life line obtained from this progressive test.

$$\tau_c = (\gamma + 1)\frac{D_c}{E_c{}^{\gamma}} \tag{11}$$

The main advantage in the use of progressive stress tests is that they do minimise the analysis problems caused by early and late failures in a typical test sample population. This methodology has been applied to a PDMS elastomer membrane by Iannarelli *et al*. [17], where the power exponent has been measured for different levels of pre-stretch. In Section 4.2, the value of γ has been measured on different volumes of electrically stressed materials where the voltage rise is changed from 0.05 V.s^{-1} up to 500 V.s^{-1}.

4. Results and discussion

4.1 Size effect

The experimental breakdowns obtained on the three different samples are presented in Figure 4, with only the electric field and active area considered as degradation variables. It appears that when the active area increases, the mean breakdown strength reduces significantly (electrical breakdown distributions are shifted to the left in Figure 4). Additionally, the slopes of the distributions are different. indicating a larger scatter in the breakdown results when the stressed volume increases.

For the area A_1, two distinct slopes are clearly identified in the distribution of the experimental breakdowns indicating the presence of two failure mechanisms (respectively noted as *mode 1* and *mode 2*). Hence, equation (5) is used with the electric field as variable and setting the number of failure causes to $N = 2$. The resulting Weibull competing failure model is inserted into equation (3) which yields to equation (12) with η_{Ei} and $\beta_{Ei}$the scale and shape parameters of the i^{th}failure mode of the reference sample.

$$U_e(A,E) = 1 - e^{-\frac{A}{A_0}\left[\left(\frac{E}{\eta_{E1}}\right)^{\beta_{E1}} + \left(\frac{E}{\eta_{E2}}\right)^{\beta_{E2}}\right]} \tag{12}$$

Parameters that best fit the experimental data are obtained using a least squares optimization method and are given in Table 2. The resulting equation (12) is represented with lines in Figure 4 for the three areas evaluated. The CFM Weibull distribution coupled to the *size effect* is found to model accurately the experimental results, which could be interpreted as a sign that different failure modes competing in the samples is a reasonable assumption. This will be further discussed in Section 3.3.

The experimental breakdown distribution obtained on the reference area A_0 is exclusively described by the first failure mechanism (*mode 1*). This failure mode is assumed to be caused by electro-mechanical instability which is acknowledged as the dominant failure mechanism of dielectric elastomer in the absence of pre-stretch [36, 37]. This assumption is supported by the results of a previous study on the same dielectric elastomer where the onset of electromechanical instability was calculated at 200 V.µm^{-1} for an unstretched material [15]. Here, the scale parameter is measured at 192 V.µm^{-1} which is a strong indication that electro-mechanical instability is the underlying failure mechanism of *mode 1*.

Table 2. Scale and shape parameters of the CFM Weibull distribution.

	Parameter	Symbol	Value	Unit
mode 1	Scale	η_{E1}	192	V.µm^{-1}
	Shape	β_{E1}	14.5	–
mode 2	Scale	η_{E2}	2316	V.µm^{-1}
	Shape	β_{E2}	2.1	–

In contrast, the experimental breakdowns on the large samples A_2 are mainly driven by the second mechanism (*mode 2*) as indicated by the slope of the distribution. When the electrode area increases, this failure mode rapidly takes over electro-mechanical instabilities as the main cause of electrical failure. To ensure that electrical failures have occurred within the dielectric layer, after testing, a small current of 1 mA is circulated between the electrodes of opposite polarities. The Joule's dissipative heat in the highly resistive breakdown pinholes leads to a local temperature increase which diffuses across the layers up to the surface of the ring, allowing its localization with the use of an infrared camera as shown in Figure 5-a. Then, the rings are cut at this precise location, and the pinholes inspected with a microscope (Figure 5-b). Despite several layers being generally damaged,

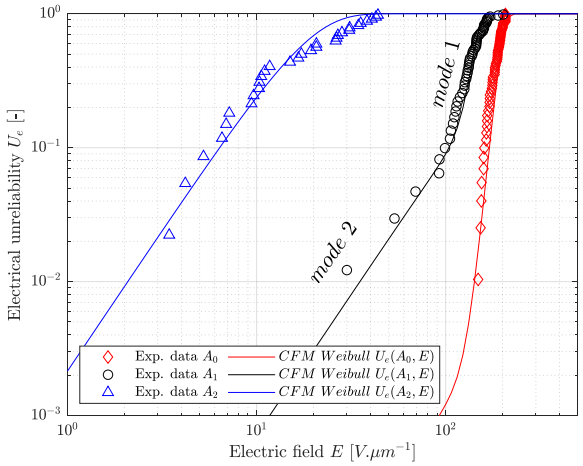

Figure 4. Experimental breakdown results modelled with a CFM Weibull distribution.

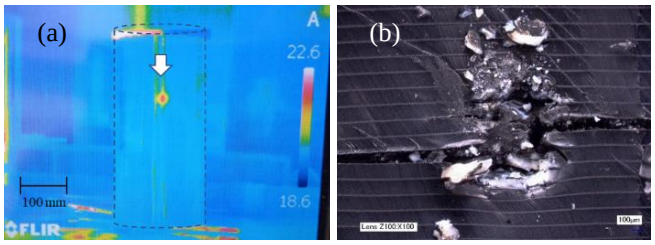

Figure 5. Breakdown pinhole inspected with (a) an infrared camera and (b) a digital microscope after cutting a slice at the location identified.

no breakdowns have been identified at electrode terminations. This observation indicates that this second failure mechanism is driven by the dielectric properties rather than electric field enhancement at the electrode tips.

Experimental breakdowns on additional intermediate areas are shown in Figure 6. Larger electrode surfaces have been coated on samples of type A_1 whereas lower dielectric layers have been stacked in sample of type A_2. These additional measurements are aimed at verifying that the reduced reliability is actually driven by a change in area rather than a change in the sample configuration. The mixed Weibull distribution (12) is represented with a colour scale, where the colour intensity increases linearly with the unreliability level. It was choosen to bound the visibility of the Weibull contour plot between 0.01 and 0.99 unreliability (dashed black lines). Large DEGs composed of a continuous piece of active material seem unrealistic for reliable operation over multiple years, and the development of segmented electrodes where each segments are interconnected with thin connections acting as fuses can be a way for improving reliability [38]. The size of these segments can be assessed based on their individual reliability, and outcome of Figure 6 gives guidelines on the typical segment area allowing for a reliable design. For the specific material and process evaluated in this study, the change of breakdown mechanism from *mode 1* to *mode 2* progressively occurred when the area increased from 10^{-2} to 10^{1} m^2. The largest area that allows 90% of the segments to survive in *mode 1* is around 10^{-1} m^2 leading to an electric field in the range of 110 V.µm^{-1} as represented by the dashed line in Figure 6. This can be defined as a critical area A_C to use as basis of design of a segmented electrode arrangement, such as the ones employed in the capacitor industry. Active surface of a unitary segment shall be preferably designed to be smaller than A_C to operate 90% of the segments away from *mode 2*.

4.2 Electrical ageing

Further to electric field and volume, the time under stress can also be added as an additional stress variable influencing the electrical reliability. Results of a progressive stress step where the voltage rise is changed from 0.05 V.s^{-1} up to 500 V.s^{-1} are represented in Figure 7 for the three geometries previously described. For the reference area A_0, the effect of exposure time is extremely limited over the time period evaluated as the mean breakdown remains unchanged for the different voltage ramps tested (Figure 7-a). For the other larger areas, electrical ageing can also be considered as marginal with regards to the size effect and is difficult to evaluate given the large scatter in the breakdown values. The CFM Weibull *cdf*, which integrates the effect of exposure time, is obtained by combining equation (7) and (5) with $N = 2$. The resulting reliability function is then inserted into equation (3) to account for the *size effect*, and the electrical unreliability function is expressed as:

$$U_e(A,E,t) = 1 - e^{-\frac{A}{A_0}\left[\left(\frac{E}{\eta_{E1}}\right)^{\beta_{E1}}\left(\frac{t}{\eta_{t1}}\right)^{\beta_{t1}}+\left(\frac{E}{\eta_{E2}}\right)^{\beta_{E2}}\left(\frac{t}{\eta_{t2}}\right)^{\beta_{t2}}\right]} \quad (13)$$

The Weibull parameters that best fit the experimental data are given in Table 3 for each failure mode, and the corresponding distribution described in equation (13) is superimposed on the experimental data for the three volumes evaluated in Figure 7. An ageing power exponent $\gamma_1 = 134$ is obtained for the smaller samples where failures are determined by *mode 1*. The very low sensitivity of electrical breakdown to exposure time supports the previous results obtained by Iannarelli *et al*. [17] on an unstretched PDMS elastomer. On the larger area, where electrical breakdowns are driven by *mode 2*, a value $\gamma_1 = 103$ is obtained. At a first glance, electrical ageing appears to be slightly enhanced as the power exponent is smaller. However, that observation has to be considered with caution due to the large scatter in the breakdown field distribution. It seems more appropriate to conclude that no major deviation in the electrical ageing kinetics occurred when the active area increases. The test duration of each individual point represented in Figure 7 never exceeded 7 days, and other ageing processes might build up at longer exposure times leading to different γ values.

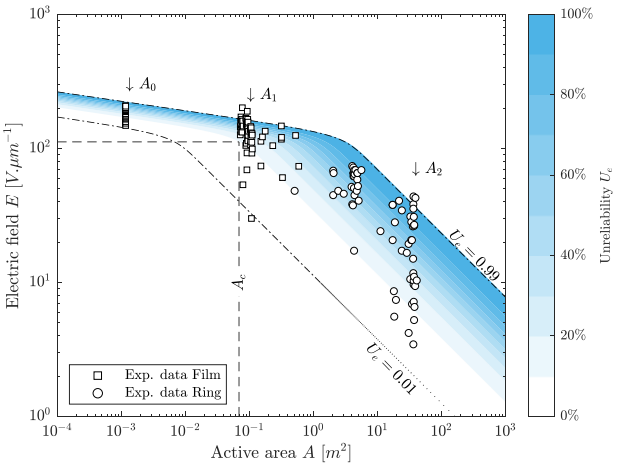

Figure 6. Electrical unreliability depending on the level of electric field and active area.

Table 3. Parameters of the inverse power law used in the CFM Weibull distribution.

	Parameter	Symbol	Value	Unit
mode 1	Scale	η_{t1}	2.0×10^4	s
	Shape	β_{t1}	0.108	–
	Power exponent	γ_1	134	–
mode 2	Scale	η_{t2}	1.3×10^9	s
	Shape	β_{t2}	0.020	–
	Power exponent	γ_2	103	–

4.3 Discussion

For improving the reliability of DEGs constituted of large areas of dielectric material, identifying and eliminating the early failures caused by *mode 2* is crucial. Microscope inspections have been performed on the dielectric films, and when a defect is identified, a breakdown test is performed at this specific location using the cylindrical stainless-steel electrode described in Section 3.2. This electrode was centered above the defect, and a voltage ramp up of 500 V.s^{-1} was applied until electrical breakdown. The breakdown strength was calculated from the initial film thickness (equation (9)) and can be compared to the values measured on a defect-free sample (Figure 7-a). After breakdown, the film was re-inspected, and breakdown pinholes were always localised on the previously identified defects (Figure 8). For the bubble-shape defects, dielectric breakdown strengths ranging from 13 to 53 V.µm^{-1} have been measured on 11 different bubbles. For the filamentary defect, the breakdown strength was higher and a value of 101 V.µm^{-1}was measured on the film (localized field enhancements are likely higher at the extremity of the defect where the breakdown occurred). For the different types of defects, the measured values are in the range of the breakdown values identified as *mode 2* in Figure 4. This tends to indicate that *mode 1* corresponds to electro-mechanical instabilities, whereas *mode 2* covers different types of flaws of variable nature and sizes, leading to premature failure and a larger dispersion in the experimental breakdowns.

These results highlight the importance of the manufacturing process in the production of large DEGs. The presence of contaminants shall be avoided with specific efforts in the material formulation and manufacturing process (such as clean room environment). The bubbles-shape defects require specific additional steps like vacuum degassing, planetary mixing, or specific disposition in the coating process. Despite all these preventive actions, it is impossible to guarantee a 100% defect free large-scale DEG. For this reason, developing stretchable electrodes with self-clearing properties or patterned electrodes would be game changers for the industrialization of dielectric elastomer transducers. The major contribution of microscopic defects to the reliability of large-scale DEGs indicates that breakthrough electrode technologies are prerequisites to the development of material formulations with higher dielectric breakdown strength or higher dielectric permittivities.

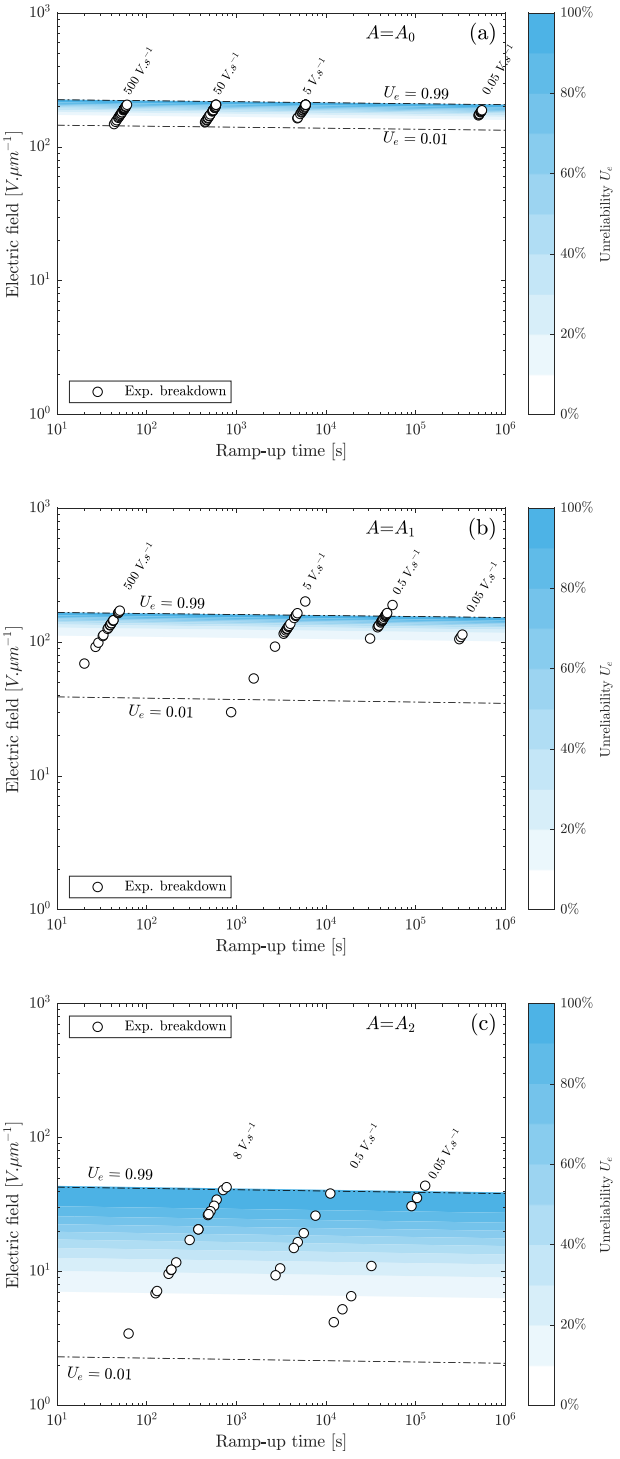

Figure 7. Electrical ageing obtained from a progressive stress test on samples with electrode areas equal to (a) $\boldsymbol{A = A_0}$, (b) $\boldsymbol{A = A_1}$ and (c) $\boldsymbol{A = A_2}$.

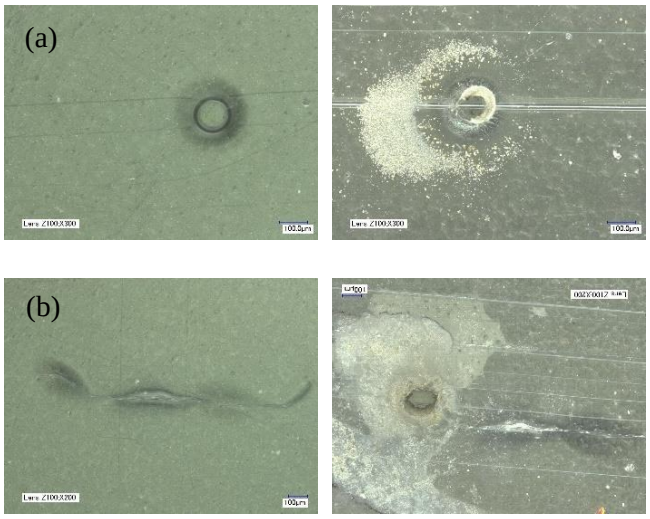

Figure 8. Microscope picture of defect before voltage application (left) and after electrical failure (right) for an air bubble (a) and a filamentary particle (b).

5. Conclusion

The electrical breakdown distribution has been measured on different sizes of dielectric materials by varying the electrode area. It was found that the presence of defects, such as air bubbles or external contaminants, significantly reduced the breakdown strength of the larger active areas. The energy density of DEGs is generally extrapolated from breakdown tests realised on relatively small-scale samples of dielectric material. In these common breakdown setups, defect-driven failure mechanisms are often hidden, causing misinterpretation of the *size effect.* However, considering several breakdown mechanisms in a Weibull competing failure model allows an accurate description of the *size effect* and electrical ageing. According to the experimental results, the *size effect* outweighed electrical ageing in determining electrical unreliability. These results highlight the importance of testing dielectric elastomers at representative scales for determining their operating limits. The power exponent of the electrical ageing law was found to be in accordance with literature for the small, non-stretched PDMS samples, and a similar sensitivity to exposure time was measured on the larger samples. For reaching commercial application on large-scale devices and operating such systems in the range of 80-100 $V.\mu m^{-1}$, the development of patterned or self-clearing electrodes is mandatory unless an extreme degree of purity can be achieved in the dielectric for the purpose of excluding any type of defect that would lead to an electrical failure before the design life of the DEG. A methodology has been proposed to evaluate the critical area at which the failure mechanism transitions from electro-mechanical instabilities to premature failures induced by defects.

Acknowlegements

This work was supported by SBM Offshore in the framework of the S3 Wave Energy Converter development. The authors would like to express their gratitude to Ronan Pin for his assistance with sample preparation and testing.

References

[1] C. Jean-Mistral, S. Basrour, and J.-J. Chaillout, "Dielectric polymer: Scavenging energy from human motion," in *The International Society for Optical Engineering*, 2008, vol. 6927,

[2] R. D. Kornbluh, J. Eckerle, and B. McCoy, "A scalable solution to harvest kinetic energy," *SPIE Newsroom*, 2011.

[3] P. Jean *et al.*, "Standing wave tube electro active polymer wave energy converter," in *SPIE Smart Structures and Materials +Nondestructive Evaluation and Health Monitoring*, 2012, vol. 8340, pp. 75-95

[4] G. Moretti *et al.*, "Advances in the development of dielectric elastomer generators for wave energy conversion," *Renewable and Sustainable Energy Reviews*, vol. 117, 2020.

[5] M. Righi, G. Moretti, D. Forehand, L. Agostini, R. Vertechy, and M. Fontana, "A broadbanded pressure differential wave energy converter based on dielectric elastomer generators," *Nonlinear Dynamics*, vol. 105, no. 4, pp. 2861-2876, 2021/09/01 2021.

[6] G. Moretti *et al.*, "Hardware-in-the-loop simulation of wave energy converters based on dielectric elastomer generators," *Meccanica*, vol. 56, no. 5, pp. 1223-1237, 2021.

[7] P. Fan, L. Zhu, Z. Zhu, H. Chen, W. Chen, and H. Hu, "Predicting energy harvesting performance of a random nonlinear dielectric elastomer pendulum," *Applied Energy*, vol. 289, p. 116696, 2021.

[8] C. Zhang, Z. Lai, X. Rao, J. Zhang, and D. Yurchenko, "Energy harvesting from a novel contact-type dielectric elastomer generator," *Energy conversion and management*, vol. 205, p. 112351, 2020.

[9] S. J. A. Koh, C. Keplinger, T. Li, S. Bauer, and Z. Suo, "Dielectric Elastomer Generators: How Much Energy Can Be Converted?," *IEEE/ASME Transactions on Mechatronics*, vol. 16, no. 1, pp. 33-41, 2011.

[10] S. J. A. Koh, X. Zhao, and Z. Suo, "Maximal energy that can be converted by a dielectric elastomer generator," *Applied Physics Letters*, vol. 94, no. 26, 2009.

[11] C. Jean-Mistral, S. Basrour, and J. J. Chaillout, "Modelling of dielectric polymers for energy scavenging applications," *Smart Materials and Structures*, vol. 19, no. 10, p. 105006, 2010/08/06 2010.

[12] S. Rosset and I. A. Anderson "Squeezing More Juice out of Dielectric Elastomer Generators," (in English), *Frontiers in Robotics and AI*, Original Research vol. 9, 2022-February-11 2022.

[13] S. Vudayagiri, S. Zakaria, L. Yu, S. Hassouneh, M. Benslimane, and A. Skov, "High breakdown-strength composites from liquid silicone rubbers," *Smart Materials and Structures*, vol. 23, p. 105017, 09/10 2014.

[14] M. Kollosche and G. Kofod, "Electrical failure in blends of chemically identical, soft thermoplastic elastomers with different elastic stiffness," *Applied Physics Letters*, vol. 96, no. 7, p. 071904, 2010.

[15] E. Taine, T. Andritsch, I. Saeedi, and P. Morshuis, "Effect of mechanical loading history on the electrical breakdown strength of dielectric elastomers," in *2022 IEEE 4th*

International Conference on Dielectrics (ICD), 2022: IEEE, pp. 21-24

[16] G. Kofod, P. Sommer-Larsen, R. D. Kornbluh, and R. Pelrine, "Actuation response of polyacrylate dielectric elastomers," *Journal of Intelligent Material Systems and Structures*, vol. 14, no. 12, pp. 787–793, 2003.

[17] A. Iannarelli, M. G. Niasar, and R. Ross, "The effects of static pre-stretching on the short and long-term reliability of dielectric elastomer actuators," *Smart Materials and Structures*, vol. 28, no. 12, p. 125014, 2019/11/08 2019.

[18] S. Zakaria, P. H. F. Morshuis, M. Y. Benslimane, L. Yu, and A. L. Skov, "The electrical breakdown strength of pre-stretched elastomers, with and without sample volume conservation," *Smart Materials and Structures*, vol. 24, no. 5, p. 055009, 2015/04/09 2015.

[19] J. Huang, S. Shian, R. M. Diebold, Z. Suo, and D. R. Clarke, "The thickness and stretch dependence of the electrical breakdown strength of an acrylic dielectric elastomer," *Applied Physics Letters*, vol. 101, no. 12, p. 122905, 2012/09/17 2012.

[20] D. Gatti, H. Haus, M. Matysek, B. Frohnapfel, C. Tropea, and H. F. Schlaak, "The dielectric breakdown limit of silicone dielectric elastomer actuators," *Applied Physics Letters*, vol. 104, no. 5, p. 052905, 2014.

[21] R. N. Hampton, A. Smedberg, and D. Wald, "Effect of size on electrical performance," *Conference Record of the 2006 IEEE International Symposium on Electrical Insulation*, pp. 25-29, 2006.

[22] B. Mazurek and J. Ranachowski, "On the size effect in the testing of breakdown voltage of PE power cables," in *1984 IEEE International Conference on Eletrical Insulation*, 1984: IEEE, pp. 58-60

[23] M. Marzinotto, C. Mazzetti, and G. Mazzanti, "A New Approach to the Statistical Enlargement Law for Comparing the Breakdown Performance of Power Cables. 1. Theory," *IEEE Transactions on Dielectrics and Electrical Insulation*, vol. 14, no. 5, pp. 1232-1241, 2007.

[24] I. Rytöluoto, K. Lahti, M. Karttunen, and M. Koponen, "Large-area dielectric breakdown performance of polymer films - part i: measurement method evaluation and statistical considerations on area-dependence," *IEEE Transactions on Dielectrics and Electrical Insulation*, vol. 22, no. 2, pp. 689-700, 2015.

[25] S. J. Laihonen, U. Gafvert, T. Schutte, and U. W. Gedde, "DC breakdown strength of polypropylene films: Area dependence and statistical behavior," *IEEE Transactions on Dielectrics and Electrical Insulation*, vol. 14, no. 2, pp. 275-286, 2007.

[26] Z. Chen *et al.*, "Prediction of Breakdown Field Strength for Large-Area and Multilayer Film Dielectrics," *IEEE Transactions on Dielectrics and Electrical Insulation*, vol. 29, no. 2, pp. 470-477, 2022.

[27] G. Moretti, S. Rosset, R. Vertechy, I. Anderson, and M. Fontana, "A review of dielectric elastomer generator systems," *Advanced Intelligent Systems*, vol. 2, no. 10, 2020.

[28] K. Di *et al.*, "Dielectric elastomer generator for electromechanical energy conversion: A mini review," *Sustainability*, vol. 13, no. 17, p. 9881, 2021.

[29] W. B. Nelson, *Accelerated testing: statistical models, test plans, and data analysis*. John Wiley & Sons, 1990.

[30] G. Chen, J. Zhao, S. Li, and L. Zhong, "Origin of thickness dependent dc electrical breakdown in dielectrics," *Applied Physics Letters*, vol. 100, no. 22, p. 222904, 2012.

[31] W. Weibull, "A Statistical Distribution Function of Wide Applicability," *Journal of Applied Mechanics*, vol. 18, no. 3, pp. 293-297, 1952.

[32] W. Wang and M. Jiang, "Competing failure or mixed failure models," in *2014 Reliability and Maintainability Symposium*, 27-30 Jan. 2014 2014, pp. 1-6

[33] K. Goda and H. Fukunaga, "The evaluation of the strength distribution of silicon carbide and alumina fibres by a multi-modal Weibull distribution," *Journal of Materials Science*, vol. 21, no. 12, pp. 4475-4480, 1986/12/01 1986.

[34] R. van Kessel, P. Bauer, and J. A. Ferreira, "Electrical modeling of cylindrical dielectric elastomer transducers," *Smart Materials and Structures*, vol. 30, no. 3, p. 035021, 2021.

[35] W. Yurkowsky, R. E. Schafer, and J. M. Finkelstein, "Accelerated testing technology," 1968.

[36] S. J. A. Koh *et al.*, "Mechanisms of large actuation strain in dielectric elastomers," *Journal of Polymer Science Part B: Polymer Physics*, vol. 49, no. 7, pp. 504-515, 2011.

[37] T. Lu, C. Ma, and T. Wang, "Mechanics of dielectric elastomer structures: A review," *Extreme Mechanics Letters*, vol. 38, p. 100752, 2020/07/01/ 2020.

[38] T. Andritsch *et al.*, "Challenges of using electroactive polymers in large scale wave energy converters," in *2012 Annual Report Conference on Electrical Insulation and Dielectric Phenomena*, 14-17 Oct. 2012 2012, pp. 786-789